Journal of Sound and Vibration (1997) **200**(1), 41–61

THE STABILITY BEHAVIOR OF A NON-CONSERVATIVE SPINNING TIMOSHENKO SHAFT WITH AN OVERHUNG DISK

L.-W. CHEN AND H.-C. SHEU

Department of Mechanical Engineering, National Cheng Kung University, Tainan 70101, *Taiwan*

(*Received* 20 *October* 1995, *and in final form* 22 *July* 1996)

The stability behavior of a spinning Timoshenko shaft with an overhung disk subjected to a follower force is analytically studied. The succinct expression of frequency (whirl speed) equations for hinged–hinged–free and clamped–hinged–free rotors are given. By using the numerical technique, the critical follower loads are sought. Numerical results reveal that the instability mechanisms are complex due to the presence of the spin speed, the overhung disk and the location of the intermediate support. Fifteen different types of instability mechanisms are presented. The critical load jump is possible when the instability mechanism changes from one to another. Furthermore, in some special cases, the critical follower loads are almost zero; therefore, such a rotor combination is extremely unstable and should be avoided for design purposes.

1. INTRODUCTION

The current trend in the design of modern rotating machinery, particularly turbomachinery, is toward the achievement of higher operating speeds. Therefore, the accurate dynamic analysis of shaft–disk (rotor) systems has become a fundamental aspect of the design of high speed turbomachines. As a result of the ever increasing demand for higher spin speeds, the shafts of the rotors are made extremely flexible, which reinforces the importance of studying the dynamics of rotor systems. There have been a number of investigations relating to this field in the past decades, as indicated in the book by Dimentberg [1] and in the survey paper by Rieger [2]. In those published studies, the main aspects of rotor dynamic behavior are the vibration due to imbalance forces and different self-excited sources, stability and torsional dynamics of shaft. However, of the many important forms of dynamic behavior of a rotor system, the most commonly predicted for design purposes are the stability regions.

In addition to torque transmission, shafts subjected to follower forces due to the pressure difference across the rotor disks can be found in many rotating machines. The study of the stability of elastic systems subjected to non-conservative forces, such as follower forces, has been of great interest in recent years. A main characteristic of such non-conservative systems is that they are mathematically non-self-adjoint. In general, there exist two types of instability mechanisms, divergence and flutter, for these problems. An excellent treatment of non-conservative stability problems of various kinds of structural components can be found in the early books by Bolotin [3] and Ziegler [4]. A comprehensive discussion of this subject with a related list of references can be found in the book by Liepholz [5].

0022–460X/97/060041 + 21 $25.00/0/sv960719

Zorii and Chernukha [6] investigated the effect of the intermediate elastic support on a column that was simply supported at one end and subjected to a follower force at the other, free one. They found an interesting effect of the transition from one instability mechanism to another: namely, if the intermediate support is close to the simply supported end the column becomes unstable by flutter; whereas if the intermediate support is far enough from the simply supported end, the column loses its stability by divergence. Elishakoff and Hollkamp [7] studied the same system of Zorii and Chernukha [6] by means of computerized symbolic algebra in conjunction with the two-mode Galerkin method. Also, in subsequent work by Elishakoff and Lottati [8], exact solutions of the same problem were presented. A general discretization method was presented by De Rosa and Franciosi [9] to analyze the effect of an intermediate support on the dynamic behavior of the previous problem. Lee [10] used the Lagrangian approach and the assumed mode method to discuss the effects of an intermediate spring support on the stability behavior of the cantilever beam. As such, it had been studied from many different points of view, by adopting the usual Euler–Bernoulli hypothesis. Quite recently, De Rosa [11] resolved the above-mentioned system by taking the shear deformation into account.

For the exact solution of a spinning Timoshenko shaft with an overhung disk subjected to a follower force, no such work has been previously investigated. The objective of this paper is to carry out the analytical forms of frequency equations of the spinning Timoshenko shaft with an overhung disk. In order to obtain a deeper insight into the dynamic behavior of a shaft–disk system, the present shaft mathematical model has taken account of rotary inertia, shear deformation, gyroscopic moments and their combined effects. The influence of the spin speed, the disk and the location of the intermediate support on instability mechanisms and their corresponding stability bounds is investigated in detail.

2. MATHEMATICAL FORMULATION

A uniform circular shaft of length L, with a thin disk attached at the right free end, support at the left end as well as at some intermediate location L_1 and spinning along its longitudinal axis at a constant speed Ω is illustrated in Figure 1. The shaft in Figure 1(a) is considered as supported by a short bearing at the left end and that in Figure 1(b) is supported by a long bearing. The bearings considered in the present study are rigid, so supported conditions can be modelled as hinged and clamped supports for short and long bearings, respectively. For the sake of convenience, the rotor as shown in Figure 1(a) will be abbreviated as H–H–F (hinged–hinged–free) rotor and that in Figure 1(b) will be abbreviated as C–H–F (clamped–hinged–free). Both rotors are subjected to a follower force that always remains normal to the disk.

The governing differential equations and corresponding boundary and continuity conditions for such an elastic system can be easily achieved by use of the extended Hamilton's principle. The equations of motion and the boundary and continuity conditions are obtained by the relation

$$\int_{t_1}^{t_2} [\delta(V - T) - \delta W]\,\mathrm{d}t = 0, \tag{1}$$

where V and T are, respectively, the strain and kinetic energies of the system, and δW is the variational work done by external forces.

In the present study, the rotor is divided into two portions, the left (from the left end to the intermediate support) and right (from the intermediate support to the free end)

portions. Two sets of inertia reference frames, $o_1x_1y_1z_1$, with origin o_1 at the left end of the rotor, and $o_2x_2y_2z_2$, with origin o_2 at the intermediate support of the rotor, are adopted. It is assumed that the axial motion is small and can be reasonably neglected, and therefore a typical cross-section of the shaft, located at a distance x_i from the origin o_i, in a deformed state, is described by the translations $v_i(x_i, t)$ and $w_i(x_i, t)$ in the y_i and z_i directions and small rotations $\beta_i(x_i, t)$ and $\gamma_i(x_i, t)$ about the y_i- and z_i-axes, where the subscript $i = 1$ and 2 designates, respectively, the left and right portions of the shaft.

Because the disk is considered to be rigid here, only the strain energy due to the shaft should be taken into consideration. Taking into account the rotatory inertia and shear deformation, the strain energy V for a shaft of cross-sectional area A and moment of inertia of the shaft cross-section I is given by

$$V = \tfrac{1}{2}\int_0^{L_1}\left\{EI\left[\left(\frac{\partial\beta_1}{\partial x_1}\right)^2+\left(\frac{\partial\gamma_1}{\partial x_1}\right)^2\right]+\kappa GA\left[\left(\frac{\partial v_1}{\partial x_1}\right)^2+\left(\frac{\partial w_1}{\partial x_1}\right)^2+\beta_1^2+\gamma_1^2\right.\right.$$

$$\left.\left.+2\frac{\partial w_1}{\partial x_1}\beta_1-2\frac{\partial v_1}{\partial x_1}\gamma_1\right]\right\}\mathrm{d}x_1+\tfrac{1}{2}\int_0^{L-L_1}\left\{EI\left[\left(\frac{\partial\beta_2}{\partial x_2}\right)^2+\left(\frac{\partial\gamma_2}{\partial x_2}\right)^2\right]\right.$$

$$\left.+\kappa GA\left[\left(\frac{\partial v_2}{\partial x_2}\right)^2+\left(\frac{\partial w_2}{\partial x_2}\right)^2+\beta_2^2+\gamma_2^2+2\frac{\partial w_2}{\partial x_2}\beta_2-2\frac{\partial v_2}{\partial x_2}\gamma_2\right]\right\}\mathrm{d}x_2. \tag{2}$$

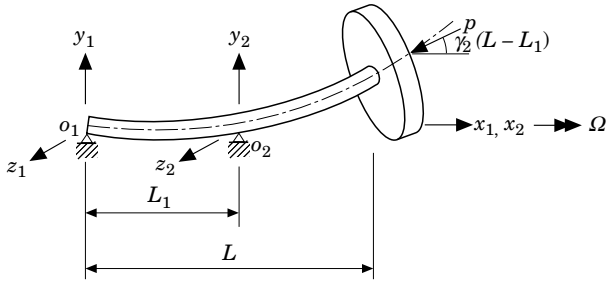

(a)

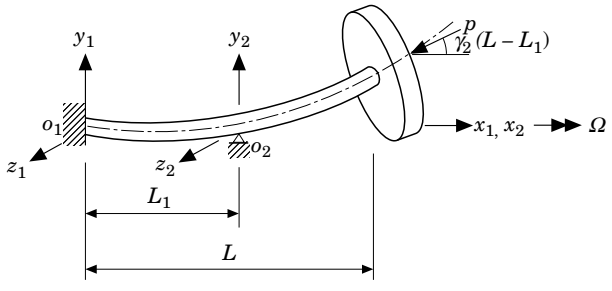

(b)

Figure 1. Spinning rotors and co-ordinate systems. (a) H–H–F rotor; (b) C–H–F rotor.

where L_1 is the distance between the left end and the intermediate support of the rotor, and E, G, ρ and κ are the Young's modulus, shear modulus, mass density and shear coefficient of the shaft respectively.

Under the assumption of constant spinning speed, the kinetic energy T of the system, including both translational and rotational forms, is given by

$$T = \tfrac{1}{2}\int_0^{L_1} \rho[A(\dot{v}_1^2 + \dot{w}_1^2) + I_d(\dot{\beta}_1^2 + \dot{\gamma}_1^2) - 2\Omega I_p\beta_1\dot{\gamma}_1 + 2\Omega^2 I_p]\,\mathrm{d}x_1$$

$$+ \tfrac{1}{2}\int_0^{L-L_1} \rho[A(\dot{v}_2^2 + \dot{w}_2^2) + I_d(\dot{\beta}_2^2 + \dot{\gamma}_2^2) - 2\Omega I_p\beta_2\dot{\gamma}_2 + 2\Omega^2 I_p]\,\mathrm{d}x_2$$

$$+ \tfrac{1}{2}[M_D(\dot{v}_2^2 + \dot{w}_2^2) + I_D(\dot{\beta}_2^2 + \dot{\gamma}_2^2) - 2\Omega I_P\beta_2\dot{\gamma}_2 + 2\Omega^2 I_P]|_{x_2 = L-L_1}, \tag{3}$$

where the superscript dot denotes differentiation with respect to time t, I_d and I_p are the diameter and polar moments of inertia per unit length of the shaft respectively, M_D is the mass of the disk, and I_D and I_P are the diameter and polar mass moments of inertia of the disk respectively. Note that $I_p = 2I_d$ and $I_d = I$ for the uniform circular shaft cross-section, and $I_P \approx 2I_D$ for the thin circular disk.

Practical rotors possess inherent external and internal damping, which tend to affect the stability behavior of the present non-conservative rotor system. However, the inclusion of external and internal damping in the present study will make the problem intractable with regard to analytical solution. Also, the instability mechanism will become more complex for the consideration of internal damping in the present study. This is because, in the absence of follower force, a rotor system may lose its stability at some spin speed due to internal damping [12]. Therefore, external and internal damping are not included in the present study. From the above, the only variational work included in this study is due to the follower force p and can be expressed as

$$\delta W = \int_0^{L_1} p\left[\frac{\partial v_1}{\partial x_1}\,\delta\left(\frac{\partial v_1}{\partial x_1}\right) + \frac{\partial w_1}{\partial x_1}\,\delta\left(\frac{\partial w_1}{\partial x_1}\right)\right]\mathrm{d}x_1$$

$$+ \int_0^{L-L_1} p\left[\frac{\partial v_2}{\partial x_2}\,\delta\left(\frac{\partial v_2}{\partial x_2}\right) + \frac{\partial w_2}{\partial x_2}\,\delta\left(\frac{\partial w_2}{\partial x_2}\right)\right]\mathrm{d}x_2$$

$$+ p(\beta_2\delta w_2 - \gamma_2\delta v_2)|_{x_2 = L-L_1}. \tag{4}$$

Upon substitution of equations (2)–(4) into the extended Hamilton's principle, equation (1), the governing differential equations for the system are obtained as follows:

$$(\kappa GA - p)\frac{\partial^2 v_i}{\partial x_i^2} - \kappa GA\frac{\partial \gamma_i}{\partial x_i} - \rho A\ddot{v}_i = 0, \tag{5}$$

$$(\kappa GA - p)\frac{\partial^2 w_i}{\partial x_i^2} + \kappa GA\frac{\partial \beta_i}{\partial x_i} - \rho A\ddot{w}_i = 0, \tag{6}$$

$$EI\frac{\partial^2 \beta_i}{\partial x_i^2} - \kappa GA\left(\frac{\partial w_i}{\partial x_i} + \beta_i\right) - 2\rho\Omega I\dot{\gamma}_i - \rho I\ddot{\beta}_i = 0, \tag{7}$$

$$EI\frac{\partial^2\gamma_i}{\partial x_i^2}+\kappa GA\left(\frac{\partial v_i}{\partial x_i}-\gamma_i\right)+2\rho\Omega I\dot{\beta}_i-\rho I\ddot{\gamma}_i=0. \tag{8}$$

The necessary and sufficient boundary and continuity conditions are found as follows: hinged end (at $x_1=0$),

$$v_1(x_1=0,t)=0,\qquad w_1(x_1=0,t)=0,\qquad \frac{\partial\beta_1(x_1=0,t)}{\partial x_1}=0,\qquad \frac{\partial\gamma_1(x_1=0,t)}{\partial x_1}=0; \tag{9}$$

clamped end (at $x_1=0$),

$$v_1(x_1=0,t)=0,\qquad w_1(x_1=0,t)=0,\qquad \beta_1(x_1=0,t)=0,\qquad \gamma_1(x_1=0,t)=0; \tag{10}$$

free end (at $x_2=L-L_1$),

$$\frac{\partial v_2(x_2=L-L_1,t)}{\partial x_2}-\gamma_2(x_2=L-L_1,t)+\frac{M_D}{\kappa GA-p}\ddot{v}_2(x_2=L-L_1,t)=0, \tag{11}$$

$$\frac{\partial w_2(x_2=L-L_1,t)}{\partial x_2}+\beta_2(x_2=L-L_1,t)+\frac{M_D}{\kappa GA-p}\ddot{w}_2(x_2=L-L_1,t)=0, \tag{12}$$

$$EI\frac{\partial\beta_2(x_2=L-L_1,t)}{\partial x_2}+I_D\ddot{\beta}_2(x_2=L-L_1,t)+2\Omega I_D\dot{\gamma}_2(x_2=L-L_1,t)=0, \tag{13}$$

$$EI\frac{\partial\gamma_2(x_2=L-L_1,t)}{\partial x_2}+I_D\ddot{\gamma}_2(x_2=L-L_1,t)-2\Omega I_D\dot{\beta}_2(x_2=L-L_1,t)=0; \tag{14}$$

continuity conditions (across $x_1=L_1$ and $x_2=0$),

$$\begin{gathered}v_1(x_1=L_1,t)=v_2(x_2=0,t)=0,\qquad w_1(x_1=L_1,t)=w_2(x_2=0,t)=0,\\ \beta_1(x_1=L_1,t)=\beta_2(x_2=0,t)=0,\qquad \gamma_1(x_1=L_1,t)=\gamma_2(x_2=0,t),\\ \frac{\partial\beta_1(x_1=L_1,t)}{\partial x_1}=\frac{\partial\beta_2(x_2=0,t)}{\partial x_2},\qquad \frac{\partial\gamma_1(x_1=L_1,t)}{\partial x_1}=\frac{\partial\gamma_2(x_2=0,t)}{\partial x_2}.\end{gathered} \tag{15}$$

Introducing the complex notation

$$u_i=v_i+\mathrm{j}w_i,\qquad \psi_i=\gamma_i-\mathrm{j}\beta_i, \tag{16}$$

and letting

$$x_i=L\xi_i,\qquad L_1/L=\eta,\qquad u_i=LU_i\,\mathrm{e}^{\mathrm{j}\omega t},\qquad \psi_i=\Psi_i\,\mathrm{e}^{\mathrm{j}\omega t}, \tag{17}$$

in which U_i and Ψ_i are the normal functions of u_i and ψ_i respectively, ξ_i is the non-dimensional length of the shaft and ω is the angular frequency.

Omitting the factor $\mathrm{e}^{\mathrm{j}\omega t}$, equations (5)–(8) become

$$(1-\bar{p}s^2)\frac{\mathrm{d}^2U_i}{\mathrm{d}\xi_i^2}+\bar{\omega}^2s^2U_i-\frac{\mathrm{d}\Psi_i}{\mathrm{d}\xi_i}=0, \tag{18}$$

$$s^2\frac{\mathrm{d}^2\Psi_i}{\mathrm{d}\xi_i^2}+[\bar{\omega}r^2s^2(\bar{\omega}-2\bar{\Omega})-1]\Psi_i+\frac{\mathrm{d}U_i}{\mathrm{d}\xi_i}=0, \tag{19}$$

where the non-dimensional coefficients are

$$\begin{gathered}r^2=I/AL^2,\qquad s^2=EI/\kappa GAL^2,\qquad \bar{p}=pL^2/EI,\\ \bar{\omega}^2=\rho AL^4\omega^2/EI,\qquad \bar{\Omega}^2=\rho AL^4\Omega^2/EI.\end{gathered} \tag{20}$$

Uncoupling U_i and Ψ_i yields the following equations:

$$\frac{d^4}{d\xi_i^4} U_i(\xi_i) + 2a \frac{d^2}{d\xi_i^2} U_i(\xi_i) + bU_i(\xi_i) = 0, \tag{21}$$

$$\frac{d^4}{d\xi_i^4} \Psi_i(\xi_i) + 2a \frac{d^2}{d\xi_i^2} \Psi_i(\xi_i) + b\Psi_i(\xi_i) = 0, \tag{22}$$

where

$$a = [\bar{\omega}^2(r^2 + s^2) - 2\bar{\omega}r^2\bar{\Omega} - \bar{p}(\bar{\omega}^2r^2s^2 - 2\bar{\omega}r^2s^2\bar{\Omega} - 1)]/[2(1 - \bar{p}s^2)], \tag{23}$$

$$b = \bar{\omega}^2[\bar{\omega}r^2s^2(\bar{\omega} - 2\bar{\Omega}) - 1]/(1 - \bar{p}s^2). \tag{24}$$

The necessary and sufficient boundary and continuity conditions for the system are also expressed in non-dimensional complex form as follows:

hinged end,

$$U_1(\xi_1 = 0) = 0, \qquad \frac{d\Psi_1(\xi_1 = 0)}{d\xi_1} = 0; \tag{25}$$

clamped end,

$$U_1(\xi_1 = 0) = 0, \qquad \Psi_1(\xi_1 = 0) = 0; \tag{26}$$

free end,

$$\frac{dU_2(\xi_2 = 1)}{d\xi_2} - \Psi_2(\xi_2 = 1 - \eta) - \frac{\bar{\omega}^2s^2\bar{M}_D}{1 - \bar{p}s^2} U_2(\xi_2 = 1 - \eta) = 0, \tag{27}$$

$$\frac{d\Psi_2(\xi_2 = 1 - \eta)}{d\xi_2} - \bar{\omega}\bar{I}_D(\bar{\omega} - 2\bar{\Omega})\Psi_2(\xi_2 = 1 - \eta) = 0, \tag{28}$$

where

$$\bar{M}_D = M_D/\rho AL, \qquad \bar{I}_D = I_D/\rho AL^3; \tag{29}$$

continuity conditions,

$$U_1(\xi_1 = \eta) = U_2(\xi_2 = 0) = 0, \qquad \Psi_1(\xi_1 = \eta) = \Psi_2(\xi_2 = 0), \qquad \frac{d\Psi_1(\xi_1 = \eta)}{d\xi_1} = \frac{d\Psi_2(\xi_2 = 0)}{d\xi_2}. \tag{30}$$

3. SOLUTIONS

With the aid of the standard procedure for solving ordinary differential equations, a quartic auxiliary equation is derived. The roots of the auxiliary equations have three possibilities; however, only two cases are practical and the other one is of a much higher frequency mode and is hence of less interest in practical application. Thus, for the sake of saving space, only the two practical cases are presented here.

Case A. Suppose that the auxiliary equation has two real and two pure imaginary roots, say $\pm\alpha_1$ and $\pm j\alpha_2$. This happens when $b < 0$, and the general solutions of U_i and Ψ_i are then

$$U_1(\xi_1) = C_1 \cosh(\alpha_1\xi_1) + C_2 \sinh(\alpha_1\xi_1) + C_3 \cos(\alpha_2\xi_1) + C_4 \sin(\alpha_2\xi_1),$$

$$\Psi_1(\xi_1) = m_1C_1 \sinh(\alpha_1\xi_1) + m_1C_2 \cosh(\alpha_1\xi_1) - m_2C_3 \sin(\alpha_2\xi_1) + m_2C_4 \cos(\alpha_2\xi_1), \tag{31}$$

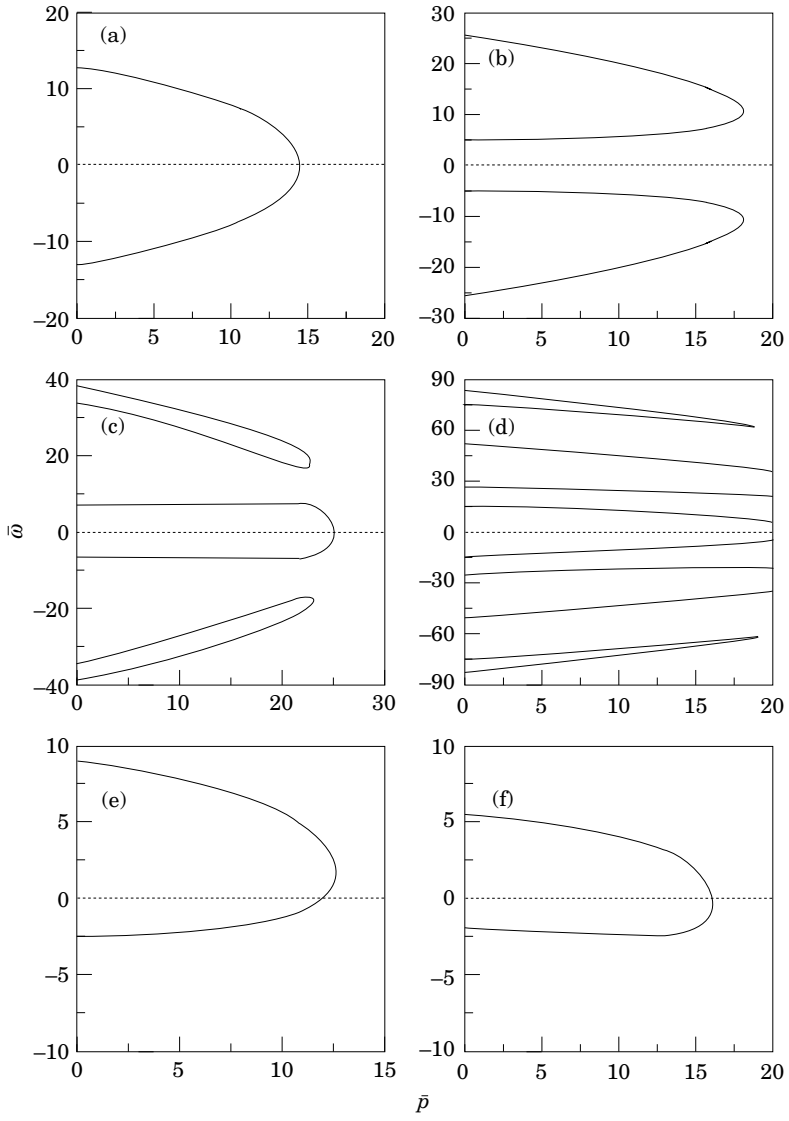

Figure 2. (a)–(f). *Caption on page* 49.

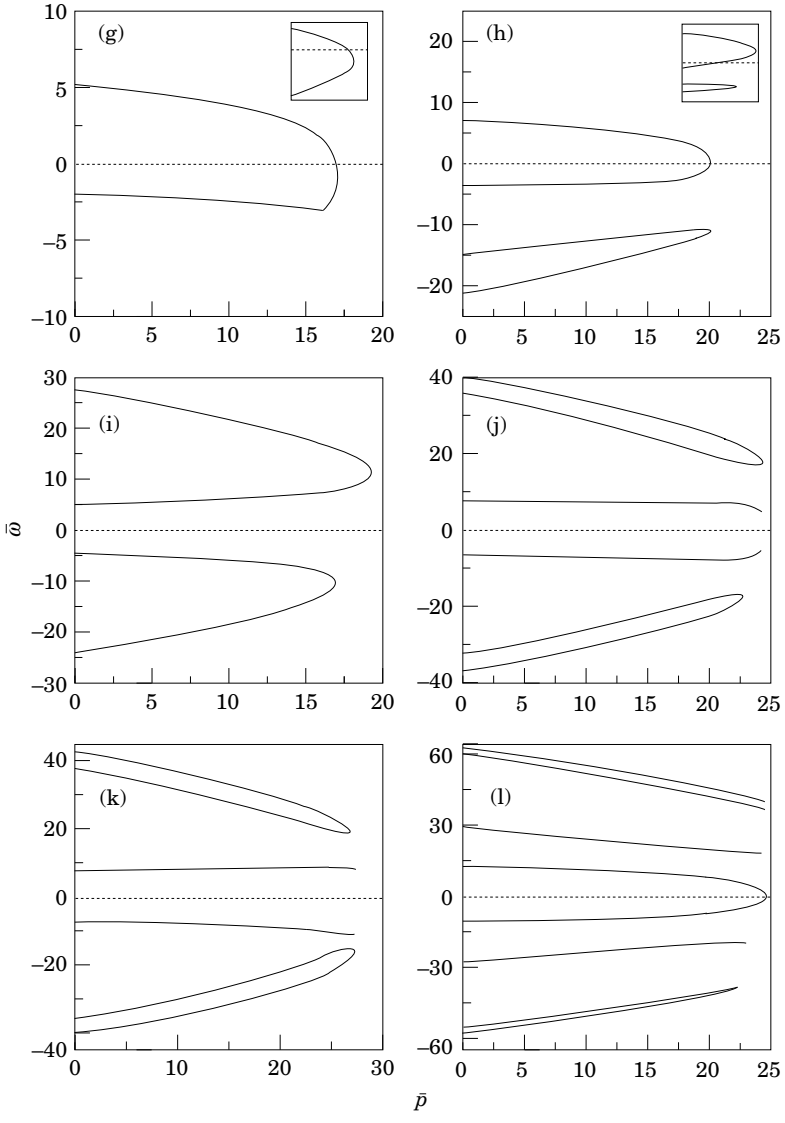

Figure 2. (g)–(l). *Caption on page* 49.

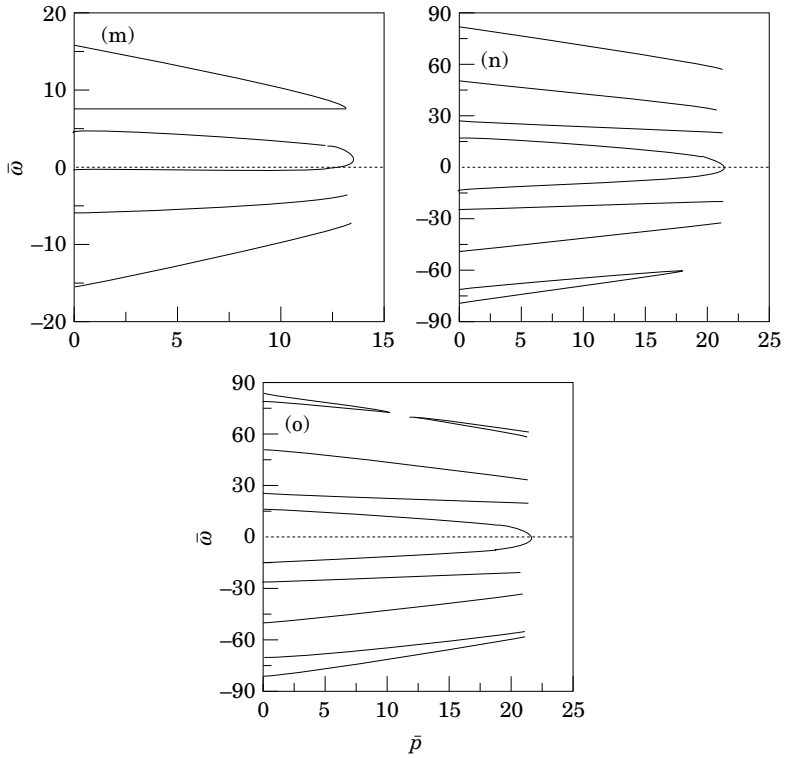

Figure 2. (m)–(o).

Figure 2. The load–frequency curves for various types of instability mechanisms. (a) H–H–F rotor, D, $\eta = 0{\cdot}7$, $\bar{\Omega} = 0$, $\bar{M}_D = 0$ and $\bar{I}_D = 0$; (b) H–H–F rotor, F12, $\eta = 0{\cdot}3$, $\bar{\Omega} = 0$, $\bar{M}_D = 0$ and $\bar{I}_D = 0$; (c) H–H–F rotor, F23, $\eta = 0{\cdot}45$, $\bar{\Omega} = 0$, $\bar{M}_D = 0$ and $\bar{I}_D = 0$; (d) C–H–F rotor, F45, $\eta = 0{\cdot}71$, $\bar{\Omega} = 0$, $\bar{M}_D = 0$ and $\bar{I}_D = 0$; (e) H–H–F rotor, F12f*, $\eta = 0{\cdot}8$, $\bar{\Omega} = 10$, $\bar{M}_D = 1$ and $\bar{I}_D = 0{\cdot}032$; (f) H–H–F rotor, D*, $\eta = 0{\cdot}6514$, $\bar{\Omega} = 10$, $\bar{M}_D = 1$ and $\bar{I}_D = 0{\cdot}032$; (g) H–H–F rotor, F12b*, $\eta = 0{\cdot}625$, $\bar{\Omega} = 10$, $\bar{M}_D = 1$ and $\bar{I}_D = 0{\cdot}032$; (h) C–H–F rotor, F12b**, $\eta = 0{\cdot}766$, $\bar{\Omega} = 5$, $\bar{M}_D = 1$ and $\bar{I}_D = 0{\cdot}032$; (i) H–H–F rotor, F12b, $\eta = 0{\cdot}3$, $\bar{\Omega} = 10$, $\bar{M}_D = 0$ and $\bar{I}_D = 0$; (j) H–H–F rotor, F23b, $\eta = 0{\cdot}45$, $\bar{\Omega} = 10$, $\bar{M}_D = 0$ and $\bar{I}_D = 0$; (k) C–H–F rotor, F23f, $\eta = 0{\cdot}49$, $\bar{\Omega} = 10$, $\bar{M}_D = 0$ and $\bar{I}_D = 0$; (l) C–H–F rotor, F34b, $\eta = 0{\cdot}63$, $\bar{\Omega} = 10$, $\bar{M}_D = 0$ and $\bar{I}_D = 0$; (m) H–H–F rotor, F34f*, $\eta = 0{\cdot}8$, $\bar{\Omega} = 3$, $\bar{M}_D = 5$ and $\bar{I}_D = 0{\cdot}8$; (n) C–H–F rotor, F45b, $\eta = 0{\cdot}72$, $\bar{\Omega} = 10$, $\bar{M}_D = 0$ and $\bar{I}_D = 0$; (o) C–H–F rotor, F45f, $\eta = 0{\cdot}71$, $\bar{\Omega} = 10$, $\bar{M}_D = 0$ and $\bar{I}_D = 0$.

$$U_2(\xi_2) = C_5 \cosh(\alpha_1\xi_2) + C_6 \sinh(\alpha_1\xi_2) + C_7 \cos(\alpha_2\xi_2) + C_8 \sin(\alpha_2\xi_2),$$

$$\Psi_2(\xi_2) = m_1 C_5 \sinh(\alpha_1\xi_2) + m_1 C_6 \cosh(\alpha_1\xi_2) - m_2 C_7 \sin(\alpha_2\xi_2) + m_2 C_8 \cos(\alpha_2\xi_2), \tag{32}$$

where

$$\alpha_1 = [-a + \sqrt{a^2 - b}]^{1/2}, \qquad \alpha_2 = [a + \sqrt{a^2 - b}]^{1/2},$$

$$m_1 = [(1 - \bar{p}s^2)\alpha_1^2 + \bar{\omega}^2 s^2]/\alpha_1, \qquad m_2 = [(1 - \bar{p}s^2)\alpha_2^2 - \bar{\omega}^2 s^2]/\alpha_2. \tag{33}$$

Case B. Suppose that the auxiliary equation has four pure imaginary roots, say $\pm j\alpha_2$

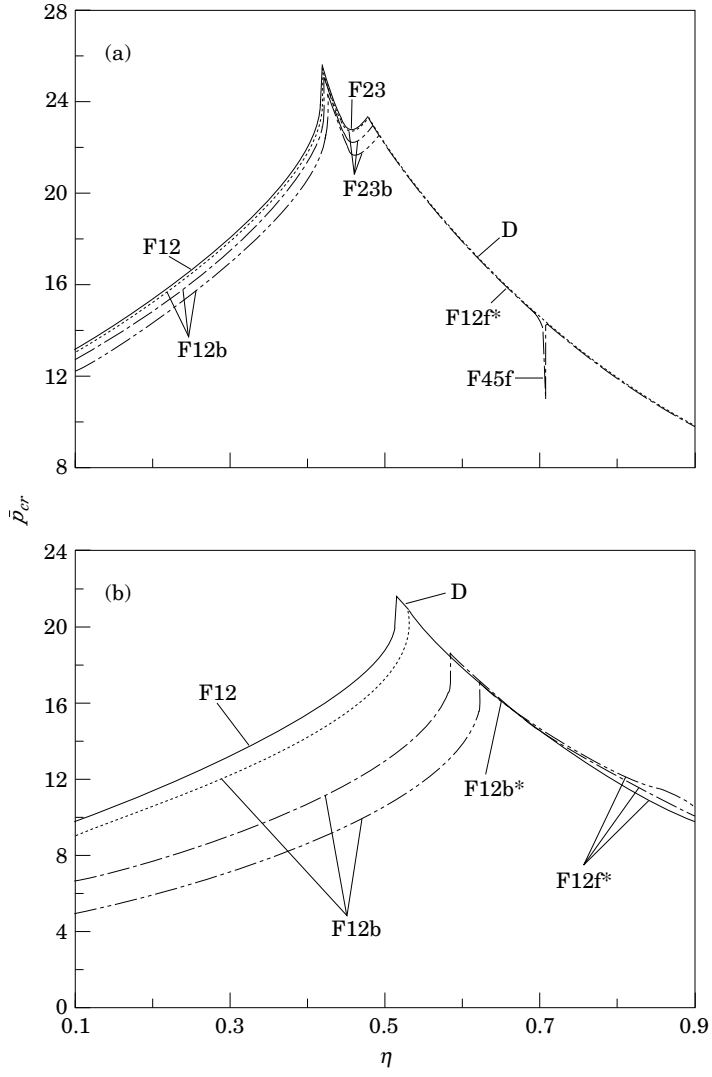

Figure 3. (a) and (b).

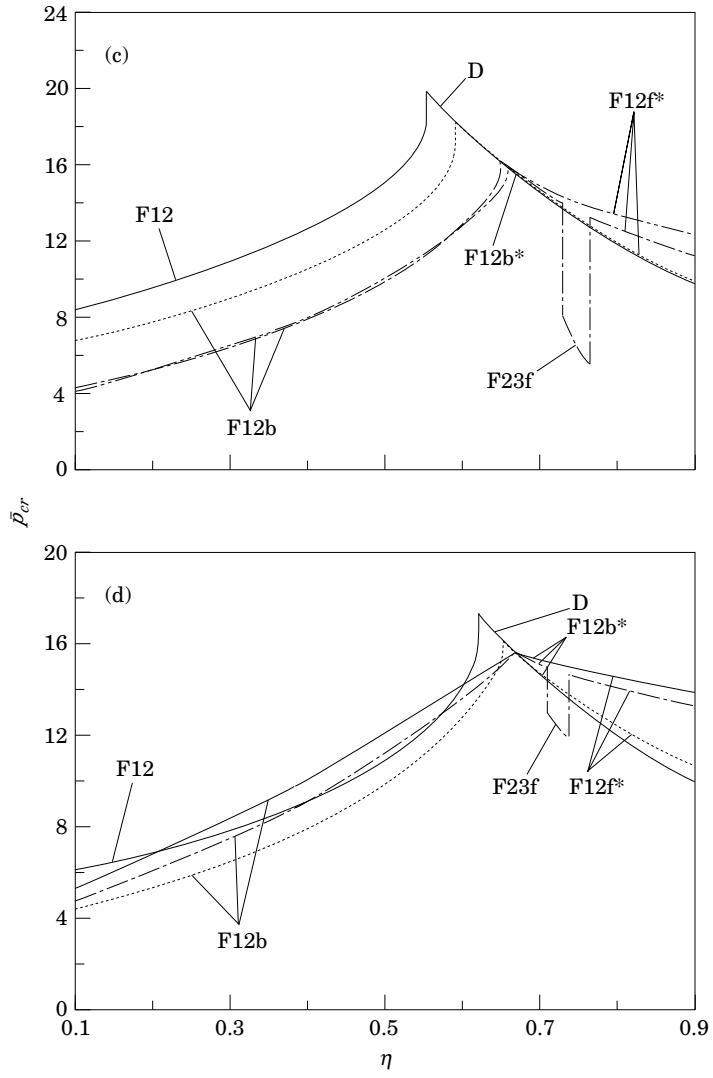

Figure 3. (c) and (d).

Figure 3. The stability boundary of the H–H–F rotor versus the location of the intermediate support. (a) $\bar{M}_D = 0$, $\bar{I}_D = 0$; (b) $\bar{M}_D = 1$, $\bar{I}_D = 0{\cdot}032$; (c) $\bar{M}_D = 2$, $\bar{I}_D = 0{\cdot}128$; (d) $\bar{M}_D = 5$, $\bar{I}_D = 0{\cdot}8$. ——, $\bar{\Omega} = 0{\cdot}0$; · · · ·, $\bar{\Omega} = 1{\cdot}0$; –·–·–, $\bar{\Omega} = 5{\cdot}0$; –··–··–, $\bar{\Omega} = 10{\cdot}0$.

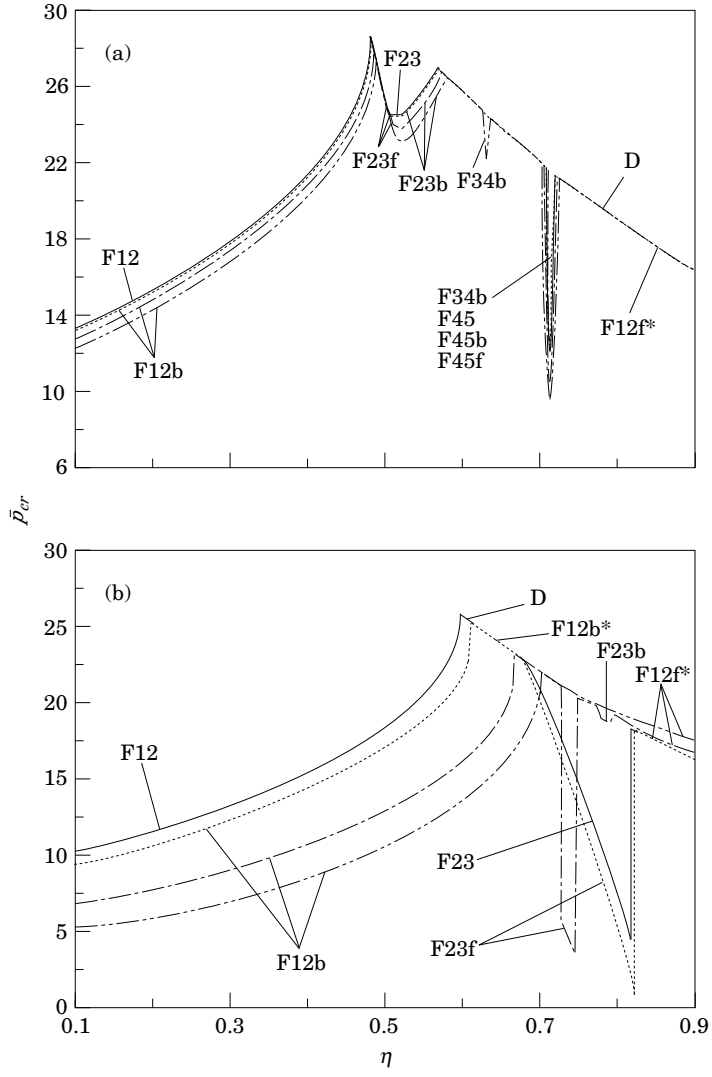

Figure 4. (a) and (b).

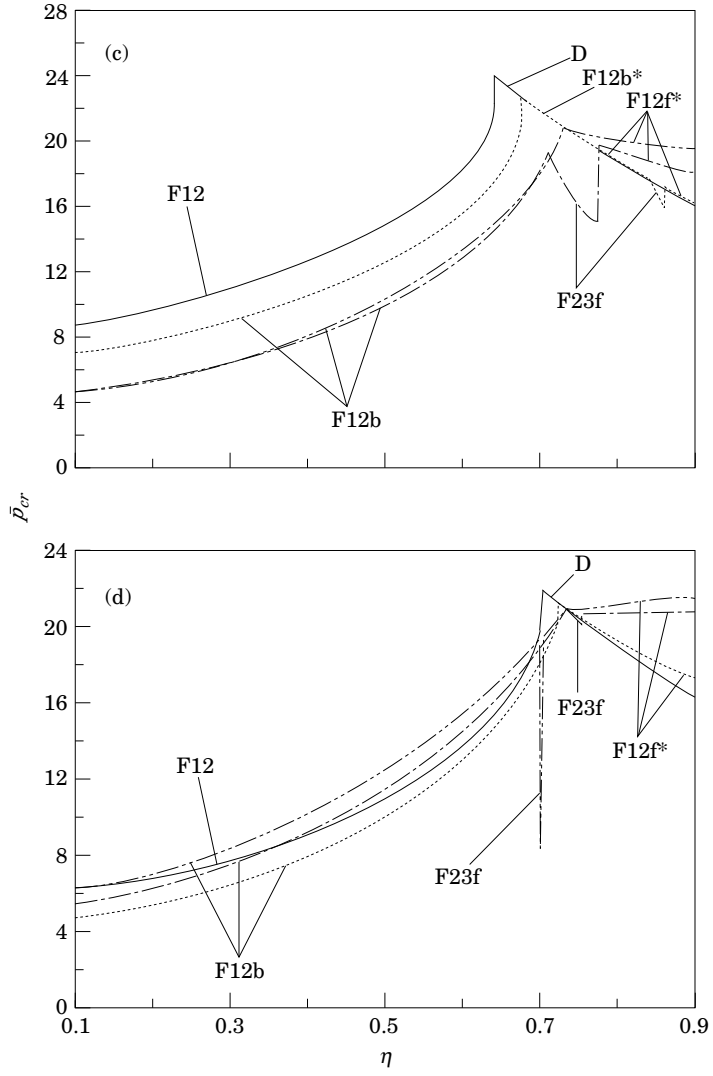

Figure 4. (c) and (d).

Figure 4. The stability boundary of the C–H–F rotor versus the location of the intermediate support. (a) $\bar{M}_D = 0$, $\bar{I}_D = 0$; (b) $\bar{M}_D = 1$, $\bar{I}_D = 0{\cdot}032$; (c) $\bar{M}_D = 2$, $\bar{I}_D = 0{\cdot}128$; (d) $\bar{M}_D = 5$, $\bar{I}_D = 0{\cdot}8$. Key as Figure 3.

and $\pm j\alpha_3$. This happens when $a^2 - b > 0$ and $b > 0$, and the general solutions of U_i and Ψ_i are then

$$U_1(\xi_1) = \bar{C}_1 \cos(\alpha_3\xi_1) + \bar{C}_2 \sin(\alpha_3\xi_1) + \bar{C}_3 \cos(\alpha_2\xi_1) + \bar{C}_4 \sin(\alpha_2\xi_1),$$
$$\Psi_1(\xi_1) = -m_3\bar{C}_1 \sin(\alpha_3\xi_1) + m_3\bar{C}_2 \cos(\alpha_3\xi_1) - m_2\bar{C}_3 \sin(\alpha_2\xi_1) + m_2\bar{C}_4 \cos(\alpha_2\xi_1), \tag{34}$$

$$U_2(\xi_2) = \bar{C}_5 \cos(\alpha_3\xi_2) + \bar{C}_6 \sin(\alpha_3\xi_2) + \bar{C}_7 \cos(\alpha_2\xi_2) + \bar{C}_8 \sin(\alpha_2\xi_2),$$
$$\Psi_2(\xi_2) = -m_3\bar{C}_5 \sin(\alpha_3\xi_2) + m_3\bar{C}_6 \cos(\alpha_3\xi_2) - m_2\bar{C}_7 \sin(\alpha_2\xi_2) + m_2\bar{C}_8 \cos(\alpha_2\xi_2), \tag{35}$$

where

$$\alpha_3 = [a - \sqrt{a^2 - b}]^{1/2}, \qquad m_3 = [(1 - \bar{p}s^2)\alpha_3^2 - \bar{\omega}^2 s^2]/\alpha_3. \tag{36}$$

The application of appropriate boundary and continuity conditions to equations (31) and (32) or equations (34) and (35) yields a set of eight homogeneous linear algebraic equations for each case. After some algebra reductions, the dimensions of the coefficient matrices become 3×3 for both cases. The elements of these coefficient matrices for each case are given in the Appendix. In order that the non-trivial solutions may exist, the determinants of coefficient matrices must be equal to zero. These lead to the frequency equation in each case from which the whirl speeds (natural frequencies) can be determined.

4. NUMERICAL RESULTS AND DISCUSSION

Elastic systems subjected to follower forces can have two types of instability: divergence (static instability) and flutter (dynamic instability). Divergence occurs when

$$\bar{\omega}_i = \bar{\omega}_j = 0 \quad (i \neq j), \qquad i, j = 1, 2, 3, \ldots, \tag{37}$$

and flutter occurs when

$$\bar{\omega}_i = \bar{\omega}_j \neq 0 \quad (i \neq j), \qquad i, j = 1, 2, 3, \ldots. \tag{38}$$

In general, the system will be referred to as unstable and its load as critical whenever a static or a dynamic instability occurs.

TABLE 1

The transition history of the types of instability mechanisms for C–H–F *rotors with* $\bar{\Omega} = 10$, $\bar{M}_D = 1$ *and* $\bar{I}_D = 0{\cdot}032$

Non-dimensional intermediate support location, η	Type of instability mechanism
0·1000–0·6670	F12b
0·6680–0·7252	F12b*
0·7253	D*
0·7254–0·7280	F12f*
0·7290–0·7480	F23f
0·7490–0·7650	F12f*
0·7660	F12b**
0·7670–0·7940	F23b
0·7950	F12b**
0·7960–0·9000	F12f*

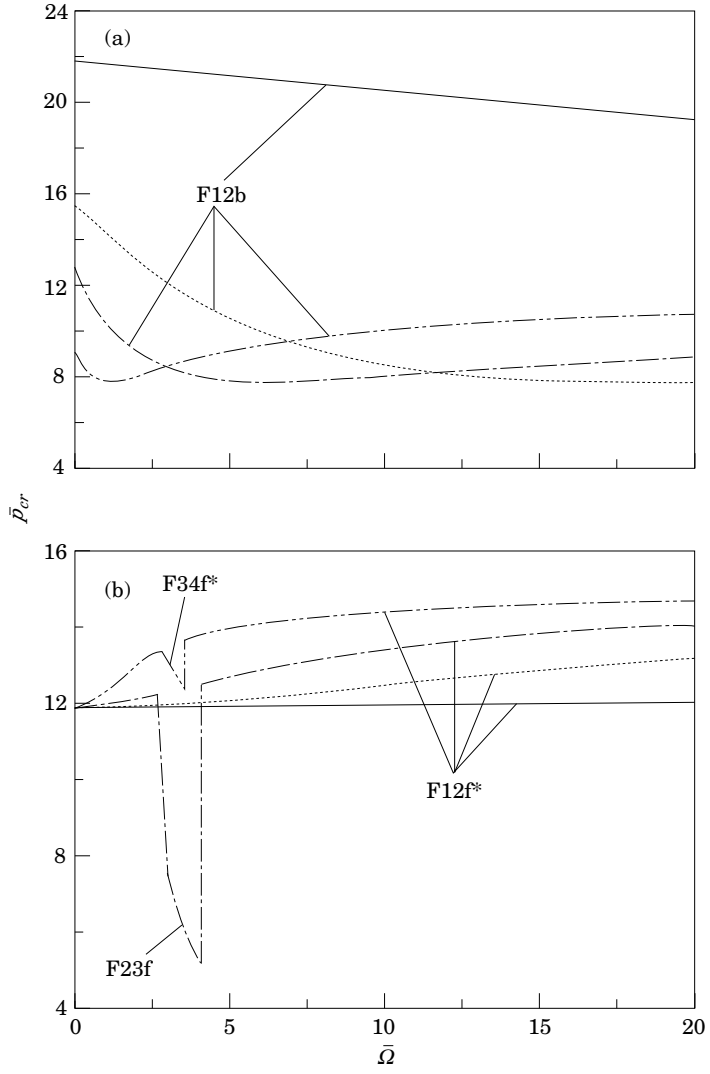

Figure 5. The stability boundary of the H–H–F rotor versus the spinning speed. (a) $\eta = 0{\cdot}4$; (b) $\eta = 0{\cdot}8$. ——, $\bar{M}_D = 0{\cdot}0$, $\bar{I}_D = 0{\cdot}0$; · · · · ·, $\bar{M}_D = 1{\cdot}0$, $\bar{I}_D = 0{\cdot}032$; –·–·–, $\bar{M}_D = 2{\cdot}0$, $\bar{I}_D = 0{\cdot}128$; –··–··–, $\bar{M}_D = 5{\cdot}0$, $\bar{I}_D = 0{\cdot}8$.

To perform the numerical simulations of the system, the basic non-dimensional data employed are the same in all discussion cases; namely $r = 0{\cdot}08$ and $E/\kappa G = 3$. For a given rotor with r, s, $\bar{M}_D$, $\bar{I}_D$, $\bar{p}$, η and $\bar{\Omega}$ known, the $\bar{\omega}_i$ ($i = 1, 2, 3, \ldots$) can be found from the appropriate frequency equations. However, these frequency equations are highly transcendental and not to be solved simply. This difficulty is overcome by the use of the numerical method. When a rotor is put into a spinning motion, its at-rest natural frequency (whirl speed) splits into two components: forward and backward precissions. In all of the figures that follow, the positive whirl speed indicates the forward precession, while the negative whirl speed denotes the backward precession. The first 12 whirl speeds (six forward and six backward modes) are considered to determine the stability bounds. However, there is no proof that the higher modes will not coalesce at an even lower follower load. It should be pointed out that the frequencies of case B, as mentioned in

the previous section, are of relatively large magnitude; however, case B should be sought in the numerical simulations because flutter may occur in the higher mode.

There exist 15 different types of instability mechanisms within the scope of the present study. These instability mechanisms are shown in detail in Figures 2(a)–(o), which demonstrate the relationships between the whirl speeds $\bar{\omega}$ and the follower force $\bar{p}$ for 15 different rotor parameters. In these figures, for the sake of convenience, a concise type name is given for each type of instability mechanism. In this scheme, "D" denotes divergence, "F" denotes flutter, "f" and "b" denote forward and backward precession, and the digits between two letters represent the coalescent modes. Furthermore, if two instability mechanisms are the same but have different load–frequency procedures, they will be distinguished by a superscript asterisk. In Figure 2(i), for example, the onset of flutter instability occurs when the two lowest backward whirl speeds coalesce; it is denoted

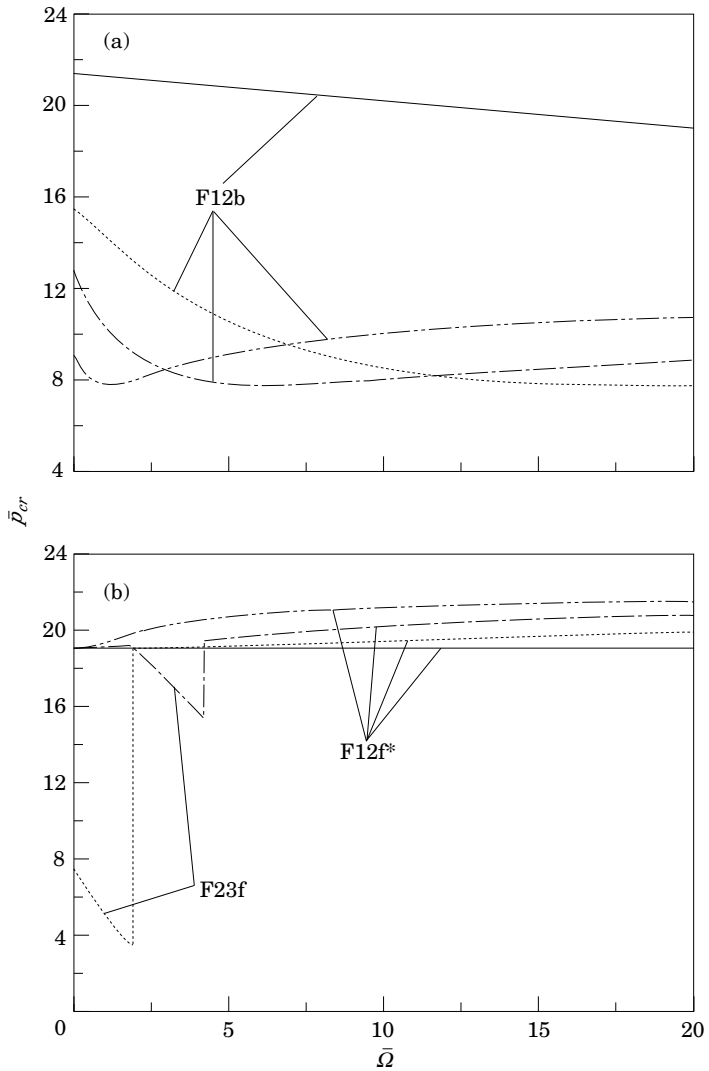

Figure 6. The stability boundary of the C–H–F rotor versus the spinning speed. (a) $\eta = 0{\cdot}4$; (b) $\eta = 0.8$. Key as Figure 5.

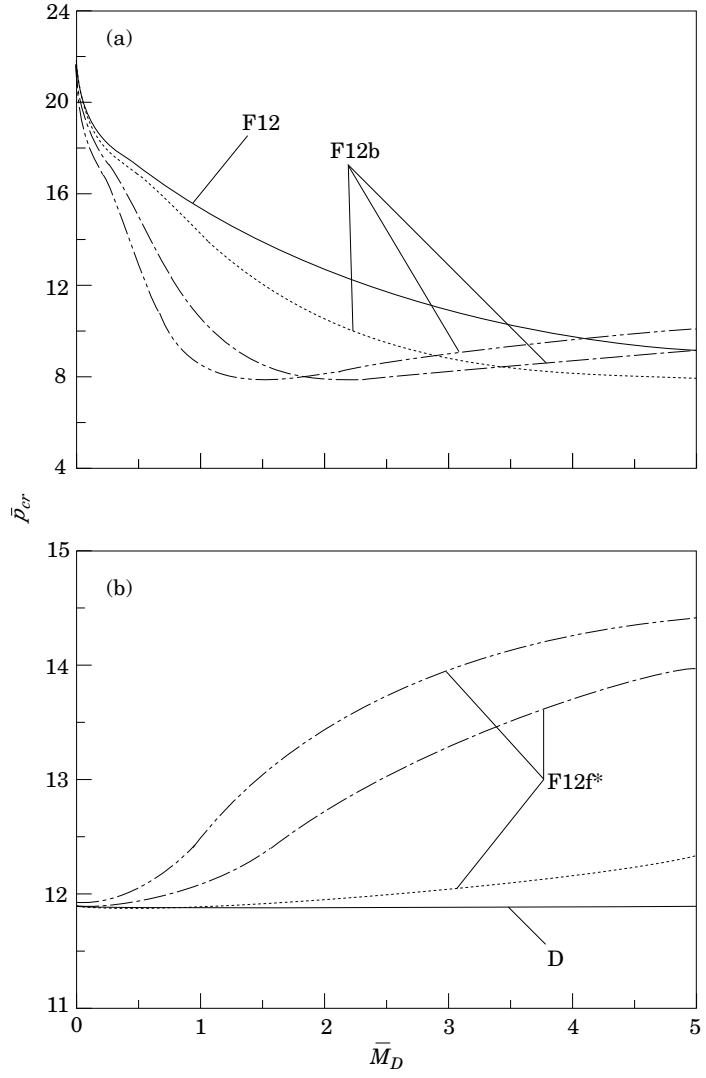

Figure 7. The stability boundary of the H–H–F rotor versus the mass and diameter mass moment of inertia of the overhung disk. (a) $\eta = 0{\cdot}4$; (b) $\eta = 0{\cdot}8$. ——, $\bar{\Omega} = 0{\cdot}0$; · · · ·, $\bar{\Omega} = 1{\cdot}0$; –·–·–, $\bar{\Omega} = 5{\cdot}0$; –··–··–, $\bar{\Omega} = 10{\cdot}0$.

as F12b. However, as shown in Figure 2(g), when the follower force slightly exceeds some value, the first forward whirl speed disappears and immediately changes its natural whirl mode to the backward manner. Since this new emergent backward whirl speed is smaller than the original first backward whirl speed, this new backward whirl speed should be denoted as the first backward mode and the original first backward whirl speed should now yield to the second backward mode. If the follower force increases continuously and sufficiently, the first two backward whirl speeds move closer and, at some value of $\bar{p}$, coincide with each other; the flutter instability occurs and this type of instability mechanism is called F12b*. The names of the other instability mechanisms can be understood in the same manner.

In Figures 3 and 4 is illustrated the influence of the location of the intermediate support on the critical follower loads of H–H–F and C–H–F rotors with four different attached

overhung disks. In each case, four spin speeds, $\bar{\Omega} = 0$, 1·0, 5·0 and 10·0, are considered. It can be observed that the instability boundaries are separated by several significant discontinuities. It is well known that if the critical load jump occurs, the accompanied change of instability mechanism is necessary. However, the converse implication is not always true. For example, when the instability mechanism transits from F12b* through D* to F12f*, the critical load curve is quite smooth, without jumping. Generally, the transition of the types of instability mechanisms of a rotor system is fairly complex. An example of a complex transition history for the instability mechanisms is shown in Table 1. An interesting observation is that the critical follower load is almost zero in Figure 4(b) for $\eta = 0{\cdot}8217$ of case $\bar{\Omega} = 1{\cdot}0$. Therefore, the rotor is extremely unstable for such a parameter combination and should be avoided for design purposes.

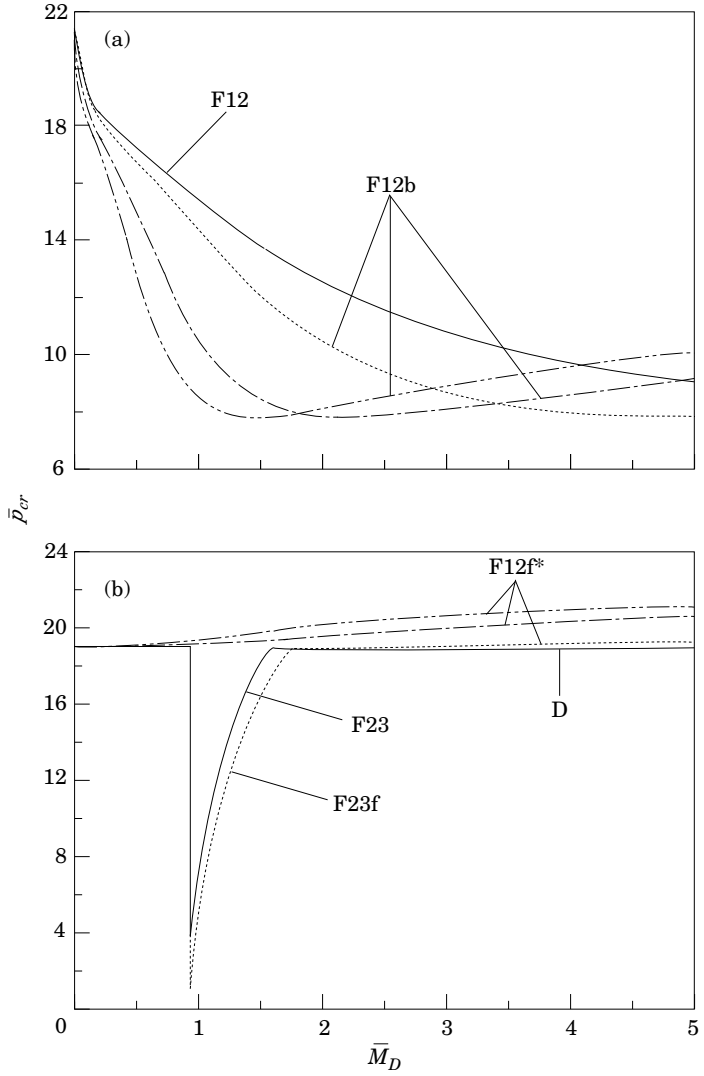

Figure 8. The stability boundary of the C–H–F rotor versus the mass and diameter mass moment of inertia of the overhung disk. (a) $\eta = 0{\cdot}4$; (b) $\eta = 0{\cdot}8$. Key as Figure 7.

The dependence of the critical follower load $\bar{p}_{cr}$ on the spin speed $\bar{\Omega}$ of the rotor system with four different attached overhung disks is studied next. Here the locations of the intermediate support is considered to be $\eta = 0{\cdot}4$ and $0{\cdot}8$, and the results are plotted in Figure 5 for an H–H–F rotor and in Figure 6 for a C–H–F rotor. It can be seen from Figures 5(a) and 6(a) that the instability mechanism is F12b for a spin speed range from 0 to 20 when $\eta = 0{\cdot}4$. As can be seen from the curves of the light disk (i.e., $\bar{M}_D = 0$, $\bar{I}_D = 0$ and $\bar{M}_D = 1{\cdot}0$, $\bar{I}_D = 0{\cdot}032$) in Figures 5(a) and 6(a), the critical follower loads are found to decrease as the spin speed increases. However, once the heavy disk (i.e., $\bar{M}_D = 2{\cdot}0$, $\bar{I}_D = 0{\cdot}128$ or $\bar{M}_D = 5{\cdot}0$, $\bar{I}_D = 0{\cdot}8$) is attached to the free end, such a tendency is not always held. The critical follower loads decrease with the spin speed at first, and at some spin speed change, to increase with spin speed. Consequently, one should be careful in drawing any conclusions about the effect of spin speed (or gyroscopic moment) on critical follower loads. In Figures 5(b) and 6(b) it is indicated that the instability mechanisms of the rotors are most probably F12f*. If only the F12f* type of instability is considered, the critical follower load increases with spin speed monotonously. As can be seen again, extremely unstable regions exist in this numerical simulation.

To examine the effect of an attached disk on the critical follower loads, the stability boundaries for H–H–F and C–H–F rotors are presented in Figures 7 and 8 respectively. Here the location of the intermediate support is again considered to be $\eta = 0{\cdot}4$ and $0{\cdot}8$. Also, for the sake of convenience, the relation between $\bar{M}_D$ and $\bar{I}_D$ is simply assumed to be $\bar{I}_D = 0{\cdot}032\bar{M}_D^2$. As observed from Figures 7(a) and 8(a), the critical follower loads decrease as the mass and diameter mass moment of inertia of the disk increase for the cases of low spin speed (i.e., $\bar{\Omega} = 0$ or $\bar{\Omega} = 1{\cdot}0$). However, once the spin speed exceeds some value (i.e., $\bar{\Omega} = 5{\cdot}0$ or $\bar{\Omega} = 10{\cdot}0$); the critical follower loads decrease with $\bar{M}_D$ and $\bar{I}_D$ first, and at some values of $\bar{M}_D$ and $\bar{I}_D$ change, to increase with $\bar{M}_D$ and $\bar{I}_D$. Upon investigation of Figure 7(b), it is seen that when the spin speed $\bar{\Omega} = 0$, the instability mechanism is divergence, and the critical load is independent of $\bar{M}_D$ and $\bar{I}_D$. This result is to be expected, since the divergence is a static phenomenon which is independent of the inertia effect. Furthermore, the critical follower loads of the F12f* type of instability increase monotonously with $\bar{M}_D$ and $\bar{I}_D$.

5. CONCLUSIONS

A stability analysis of a non-conservative spinning Timoshenko shaft with an overhung disk is presented. The succinct frequency equations for two types of shaft–disk systems have been derived by the analytical method. From the formulation and the results of the numerical simulations, the following conclusions can be drawn.

(1) Due to the effects of the spin speed, the overhung disk and the intermediate support, the instability mechanisms become more complex.

(2) Usually, the occurrence of flutter is accompanied by the coalescence of the lowest two rotor's forward or backward modes. However, higher modes may sometimes be involved in some rotor combination. If a numerical method (such as the finite element method) is used for the analysis, the same precession for the treatment of higher modes, which may cause the instability, must keep as for lower modes. The present analytical model does not have this drawback.

(3) The critical load jump is possible when the instability mechanism transits from one to another. Thus the critical load curve becomes discontinuous and its tendency is hard to predict.

(4) In some special cases, the critical follower loads are almost zero; therefore, such

parameter combinations of the rotor systems are extremely unstable and should be avoided for design purposes.

(5) As mentioned before, the internal and external damping tend to affect the instability behavior of the gyroscopic non-conservative system. It is important and challenging to investigate the effects of external and internal damping on the stability behavior of the present rotor system. This may be studied by the use of the finite element method.

REFERENCES

1. F. M. Dimentberg 1961 *Flexural Vibrations of Rotating Shafts*. London: Butterworth.
2. N. F. Rieger 1977 *Mechanism and Machine Theory* **12**, 261–270. Rotor–bearing dynamics—state-of-the-art.
3. V. V. Bolotin 1963 *Nonconservative Problems of the Theory of Elastic Stability*. New York: Pergamon Press.
4. H. Ziegler 1977 *Principles of Structural Stability*. Basel: Birkhäuser Verlag; second edition.
5. H. Leipholz 1980 *Stability of Elastic Systems*. Alphen aan der Rÿn: Sijthoff & Noordhoff.
6. L. M. Zorii and Yu. A. Chernukha 1971 *Priklady Meckhaniki Nauk* **7**, 134–136. Influence of supports on the dynamic stability of elastic column.
7. I. Elishakoff and J. Hollkamp 1987 *Computer Methods in Applied Mechanics and Engineering* **62**, 27–46. Computerized symbolic solution for a nonconservative system in which instability occurs by flutter in one range of a parameter and by divergence in another.
8. I. Elishakoff and I. Lottati 1988 *Computer Methods in Applied Mechanics and Engineering* **66**, 241–250. Divergence and flutter of nonconservative systems with intermediate support.
9. M. A. De Rosa and C. Franciosi 1990 *Journal of Sound and Vibration* **137**, 107–115. The influence of an intermediate support on the stability behaviour of cantilever beams subjected to follower forces.
10. H. P. Lee 1995 *International Journal of Solids and Structures* **32**, 1371–1382. Divergence and flutter of a cantilever rod with an intermediate spring support.
11. M. A. De Rosa 1994 *Journal of Sound and Vibration* **176**, 333–340. Exact stability analysis of combined flutter–divergence systems in the presence of shear deformation.
12. L. W. Chen and D. M. Ku 1991 *Finite Elements in Analysis and Design* **9**, 169–176. Analysis of whirl speeds of rotor–bearing systems with internal damping by C^0 finite elements.

APPENDIX: ELEMENTS OF THE MATRICES FOR HINGED–HINGED–FREE AND CLAMPED–HINGED–FREE ROTORS

Case A: $b < 0$.

$$A_{11} = \begin{cases} \dfrac{h_1 \cosh(\eta\alpha_1)\sin(\eta\alpha_2) - \sinh(\eta\alpha_1)\cos(\eta\alpha_2)}{\sinh(\eta\alpha_1)\sin(\eta\alpha_2)}, & \text{for H–H–F rotor;} \\ \dfrac{2h_1[1-\cosh(\eta\alpha_1)\cos(\eta\alpha_2)] + (h_1^2-1)\sinh(\eta\alpha_1)\sin(\eta\alpha_2)}{h_1\cosh(\eta\alpha_1)\sin(\eta\alpha_2) - \sinh(\eta\alpha_1)\cos(\eta\alpha_2)}, & \text{for C–H–F rotor,} \end{cases}$$

$$A_{12} = -h_1, \qquad A_{13} = -1,$$

$$A_{21} = h_3 \sinh[(1-\eta)\alpha_1] + h_5 \sin[(1-\eta)\alpha_2] - h_7 \cosh[(1-\eta)\alpha_1] + h_7 \cos[(1-\eta)\alpha_2],$$

$$A_{22} = h_3 \cosh[(1-\eta)\alpha_1] - h_7 \sinh[(1-\eta)\alpha_1],$$

$$A_{23} = h_5 \cos[(1-\eta)\alpha_2] - h_7 \sin[(1-\eta)\alpha_2],$$

$$A_{31} = h_1 h_5 \cosh[(1-\eta)\alpha_1] + \cos[(1-\eta)\alpha_2] - h_1 h_9 \sinh[(1-\eta)\alpha_1] - h_9 \sin[(1-\eta)\alpha_2],$$

$$A_{32} = h_1\{h_5 \sinh[(1-\eta)\alpha_1] - h_9 \cosh[(1-\eta)\alpha_1]\},$$

$$A_{33} = -\sin[(1-\eta)\alpha_2] - h_9 \cos[(1-\eta)\alpha_2],$$

where

$$h_1 = m_1/m_2, \qquad h_3 = (\bar{p}\alpha_1^2 - \bar{\omega}^2)/(\bar{p}\alpha_2^2 + \bar{\omega}^2), \qquad h_5 = \alpha_1/\alpha_2,$$

$$h_7 = \frac{\bar{\omega}^2\alpha_1\bar{M}_D}{(1-\bar{p}s^2)(\bar{p}\alpha_2^2+\bar{\omega}^2)}, \qquad h_9 = \frac{\bar{I}_D\bar{\omega}(\bar{\omega}-2\bar{\Omega})}{\alpha_2}.$$

Case B: $a^2 - b > 0$ and $b > 0$.

$$\bar{A}_{11} = \begin{cases} \dfrac{\sin(\eta\alpha_3)\cos(\eta\alpha_2) - h_2\cos(\eta\alpha_3)\sin(\eta\alpha_2)}{\sin(\eta\alpha_2)\sin(\eta\alpha_3)}, & \text{for H–H–F rotor;} \\ \dfrac{2h_2[\cos(\eta\alpha_2)\cos(\eta\alpha_3) - 1] + (h_2^2+1)\sin(\eta\alpha_2)\sin(\eta\alpha_3)}{h_2\cos(\eta\alpha_3)\sin(\eta\alpha_2) - \sin(\eta\alpha_3)\cos(\eta\alpha_2)}, & \text{for C–H–F rotor,} \end{cases}$$

$$\bar{A}_{12} = h_2, \qquad \bar{A}_{13} = 1,$$

$$\bar{A}_{21} = h_4\sin[(1-\eta)\alpha_3] - h_6\sin[(1-\eta)\alpha_2] + h_8\cos[(1-\eta)\alpha_3] - h_8\cos[(1-\eta)\alpha_2],$$

$$\bar{A}_{22} = -h_4\cos[(1-\eta)\alpha_3] + h_8\sin[(1-\eta)\alpha_3],$$

$$\bar{A}_{23} = -h_6\cos[(1-\eta)\alpha_2] + h_8\sin[(1-\eta)\alpha_2],$$

$$\bar{A}_{31} = h_2h_6\cos[(1-\eta)\alpha_3] - \cos[(1-\eta)\alpha_2] - h_2h_9\sin[(1-\eta)\alpha_3] + h_9\sin[(1-\eta)\alpha_2],$$

$$\bar{A}_{32} = h_2\{h_6\sin[(1-\eta)\alpha_3] + h_9\cos[(1-\eta)\alpha_3]\},$$

$$\bar{A}_{33} = \sin[(1-\eta)\alpha_2] + h_9\cos[(1-\eta)\alpha_2],$$

where

$$h_2 = m_3/m_2, \qquad h_4 = (\bar{p}\alpha_3^2 + \bar{\omega}^2)/(\bar{p}\alpha_2^2 + \bar{\omega}^2), \qquad h_6 = \alpha_3/\alpha_2,$$

$$h_8 = \frac{\bar{\omega}^2\alpha_3\bar{M}_D}{(1-\bar{p}s^2)(\bar{p}\alpha_2^2+\bar{\omega}^2)}.$$